Supplementary Information

In silico exploration of amyloid-related imaging abnormalities in the gantenerumab open-label extension trials using a semi-mechanistic model

Roxana Aldea, Hans Peter Grimm, Ronald Gieschke, Carsten Hofmann, Dominik Lott, Szofia Bullain, Paul Delmar, Gregory Klein, Marco Lyons, Fabrizio Piazza, Roxana O. Carare, Norman A. Mazer

Participant data

The ARIA-E vascular wall disturbance (VWD) model was designed as a semi-mechanistic pharmacokinetic-pharmacodynamic (PKPD) model. The data used for model development consists of longitudinal measurements of drug concentration in plasma and of ARIA-E magnitude from a subset of individuals who developed ARIA-E during the open label extensions (OLE) of the SCarlet Road (SR) and Marguerite Road (MR) phase III trials. The 112 individuals included in the model were all the study participants that experienced their first ARIA-E, i.e. had a BGTS > 0, within one year after the first dose of gantenerumab in the OLE period, as of 29 May 2018. For simplicity, the individuals that experienced ARIA-E only in their second year of treatment were not included in the model. Each individual was treated with subcutaneously administered gantenerumab and was assigned to one of the five dose titration regimens shown in Supplementary Table 1. The ARIA-E magnitude was quantified with the Barkhof Grant Total Score (BGTS), which is an integer between 0 and 60, with BGTS = 0 indicating the absence of ARIA-E. The reported BGTS accounted for the number and size of parenchymal hyperintensities, sulcal hyperintensities and gyral swelling present on FLAIR images [1,2].

In SR/MR OLEs, during the titration phase, routine MRI monitoring was performed before each titration step and on a study-specific routine basis after target dose was reached. More frequent MRI monitoring was performed at the investigators discretion and also if ARIA-E was identified until its resolution. Dose interventions occurred for any symptomatic ARIA-E case and for asymptomatic ones with BGTS>=4.

PK model

The purpose of the pharmacokinetic (PK) model is to capture the observed time course of gantenerumab concentration in plasma and to simulate continuous concentration-time courses. Using the gantenerumab population PK model recently developed by others [3], individual PK parameters for the ARIA-E cases from SR/MR OLE were estimated with a Bayesian approach (Monolix Suite 2020R1). This estimation made use of the individual drug dosage and longitudinal observations of drug concentration in plasma. It is noted that the SR/MR OLE studies included higher doses than the earlier gantenerumab studies that were used to develop the population PK model. Supplementary Figure 1 indicates that the previously built population PK model was able to describe the individual PK data from the SR/MR OLE studies: the residuals are evenly distributed around zero with most values within -2 and +2 standard deviations, thereby indicating no major systemic bias.

PD model

The pharmacodynamic (PD) model relates the gantenerumab exposure to ARIA-E observations via the intermediate steps of gantenerumab-driven changes in the levels of local amyloid-β ($A\beta$) and VWD. Therefore, the ARIA-E cases seen on placebo cannot be explained with the VWD model. The rate of drug-mediated removal of local $A\beta$ is assumed to depend on the product of drug concentration in plasma $Cp(t)\left[\frac{mcg}{ml}\right]$ and the level of local $A\beta(t)$ [arbitrary units] via the parameter $\alpha_{removal}\left[\left(day\cdot\frac{mcg}{ml}\right)^{-1}\right]$:

$$\frac{dA\beta(t)}{dt} = -\alpha_{removal}\cdot Cp(t)\cdot A\beta(t), \qquad (1)$$

where t is the time and the initial value of local $A\beta$ at the start of the OLE treatment (i.e. $A\beta(t=0)$) is $Amyloid_0$.

The removal of local $A\beta$ drives the build-up of $VWD(t)$ [arbitrary units], which is counter-acted by a first-order vascular repair process with the repair rate constant k_{repair} $[day^{-1}]$) and half-life independent of the VWD magnitude:

$$\frac{dVWD(t)}{dt} = \alpha_{removal}\cdot Cp(t)\cdot A\beta(t) - k_{repair}\cdot VWD(t), \qquad (2)$$

where the initial value of VWD at the start of the OLE treatment (i.e. $VWD(t=0)$) is assumed to be zero.

Next, VWD needs to be connected to the observed ARIA-E magnitude. However, the large number of zero BGTS values from the dataset of ARIA-E scores brings on computational complications that were addressed with a two-part model [4]. The first part deals with the probability $p(t)$ of a positive (non-zero) BGTS under the assumption that the logarithm of the odds ratio is linearly related to $VWD(t)$ by

$$ln\left(\frac{p(t)}{1-p(t)}\right) = \beta_1\cdot\left(VWD(t) - VWD_{50}\right), \qquad (3)$$

where β_1 denotes the linear factor and the parameter VWD_{50} represents the value of $VWD(t)$ that generates a 50% probability of a positive BGTS. The second part quantifies the BGTS magnitude by using the sigmoidal response function

$$BGTS(t) = BGTS_{max}\cdot\frac{\left(\frac{VWD(t)}{EG50}\right)^{pow}}{1+\left(\frac{VWD(t)}{EG50}\right)^{pow}}, \qquad (4)$$

where $BGTS_{max}$represents the maximum ARIA-E score and $EG50$ [arbitrary units] represents the value of $VWD(t)$ leading to half-maximal BGTS. Moreover, pow is the slope factor that gives the sensitivity of response to VWD by determining the steepness of the VWD-BGTS curve (shown in Figure 1 in the main text). The two parts of the model use different types of data: for part one, all the BGTS observations are

transformed to Boolean data that indicates whether the observed BGTS is zero or positive, while for part two, the BGTS observations are restricted to the strictly positive values.

Parameter estimation

The PD parameters were estimated by fitting the PD model to the collective set of longitudinal BGTS observations, while keeping the individual PK parameters fixed. The Boolean data from the first part (e.g. YES/NO for ARIA-E occurrence) and the continuous observations from the second part (e.g. the BGTS values within the [1,60] range for ARIA-E magnitude) were implemented in the data file as two distinct observation types and modelled simultaneously. The parameter estimation was conducted with the nonlinear mixed effects method from Monolix (version 2020R1).

The parameters $Amyloid_0$, $\alpha_{removal}$ and k_{repair} were assumed to have log-normal inter-individual variability and their typical value (fixed effect) and the width of the distribution (random effect) were estimated. The parameters β_1, VWD_{50} and pow were estimated without any inter-individual variability (i.e. as fixed effects only). It can be shown that $VWD(t)$ is proportional to $Amyloid_0$, implying that the parameters $Amyloid_0$ and EG_{50} effectively appear only as a ratio in the expression for $BGTS(t)$. Therefore, to ensure structural identifiability, EG_{50} was set to one, without any loss of generality. Moreover, the value of $BGTS_{max}$ was fixed to 60, in line with the limit of the 60-point BGTS severity scale. The residual (unexplained) variability that describes the difference between observed and predicted BGTS was assumed to be independent of the predictions and to be normally distributed. The estimated population parameters (typical values and inter-individual variability) are shown in Supplementary Table 2. The diagnostic plots from Supplementary Figure 2 demonstrate the ability of the model to predict the probability of an ARIA-E event at the population level, as well as the magnitude of ARIA-E, in particular at the individual level: the residuals over time are evenly centered around zero, without a major systemic bias and with most values within -2 and +2 standard deviations.

The impact of the following patient characteristics on the distribution of random effects was assessed: age, APOE ε4 carrier status (non-carrier, homozygous, heterozygous), type of double-blind treatment (placebo, active) and the presence/absence of cerebrovascular pathology (ARIA-H and white matter hyperintensities) at the start of OLE treatment. Graphical evaluation did not reveal any strong dependency of random effects on these patient characteristics. A more detailed covariate analysis with a refined VWD model will require observations from a broader population and the inclusion of non-ARIA-E individuals. Although the assessed baseline patient characteristics did not explain the variability in the time-course of ARIA-E, they may prove more relevant for assessing the general risk of ARIA-E. For instance, based on a hazard model, others reported that study participants in gantenerumab and aducanumab studies were more likely to be at risk of an ARIA-E event if they were APOE ε4 carriers [3,5,6].

Exploration of the influence of key model parameters in the dynamics of ARIA-E

Upon model fitting to the longitudinal PK and BGTS observations, the influence of key model parameters on the evolution of ARIA-E was explored with individual-level simulations. These simulations used the set

of parameters estimated for one of the ARIA-E cases illustrated in section 3 in the main text. In order to also demonstrate the ability of the model to relate treatment adjustments to ARIA-E severity, the simulations include a simple adaptive design for dosing and MRI monitoring, as follows: (i) dose according to a specified dosing regimen; (ii) perform BGTS assessment at pre-defined times and suspend dosing when BGTS thresholds are reached, as per SR/MR OLE protocol [7]; (iii) perform BGTS assessment (every 4 weeks) during dose suspension until BGTS = 0; (iv) restart treatments at the same dose as the one prior to treatment interruption. For illustration purposes, this adaptive design created for simulations was less complex than the one used in the SR/MR OLE studies given that the latter also accounted for factors that are missing from the VWD model, such as the radiological severity of ARIA-H and/or the presence of symptoms [7].

Supplementary Discussion

The relative contribution of the two forms of Aβ aggregates to the amyloid PET signal has been a matter of debate. Some studies concluded that amyloid PET can detect vascular Aβ in CAA [8,9], while, recently, McCarter et al. reported that the amyloid PET signal is largely driven by parenchymal amyloid plaques and does not appear to be significantly confounded by CAA [10]. The latter findings are limited by the fact that only half of the subjects met the clinical diagnosis of probable CAA with a median number of two cerebral microbleeds, despite the pathological confirmation of CAA in all subjects [10]. Of note, a decade ago, the Alzheimer's Association Research Roundtable Workgroup recommended that individuals with more than four cerebral microhemorrhages at baseline MRI should not be included in anti-amyloid clinical trials [11]. Therefore, the contribution of vascular Aβ aggregates to the PET signal in clinically more severe CAA cases, in particular in those enrolled in more recent anti-amyloid studies, remains to be determined. In order to further clarify the relative risk of ARIA associated with the regional load of vascular amyloid and its removal, more analyses that integrate longitudinal PET and MRI data from anti-amyloid trials and quantify the regional distribution of the amyloid signal, FLAIR hyperintensities and CAA imaging markers are needed. Future biomarkers that are able to better distinguish between the vascular and parenchymal amyloid burden will help refine the VWD model, which could then predict the evolution of ARIA-E in patients with various degrees of AD pathology (based on the parenchymal amyloid burden) and CAA (based on the vascular amyloid burden) [12–15]. Real world data on the safety of anti-amyloid therapies and from cohorts of patients with spontaneous ARIA, such as those with CAA-related inflammation, could eventually become an insightful source of such biomarkers.

Supplementary Table 1. Up-titration regimens for OLE in the SR and MR phase III trials

#	Day 1	Week 4	Week 8	Week 12	Week 16	Week 20	Week 24-28	Week 32-36	Week 40-100
1	105	105	105	225	225	225	450	900	1200
2	225	225	450	450	900	900	1200	1200	1200
3	300	300	600	600	1200	1200	1200	1200	1200
4	450	450	900	900	1200	1200	1200	1200	1200
5	600	600	1200	1200	1200	1200	1200	1200	1200

All the doses shown for the five regimens are in milligrams (mg).

Supplementary Table 2. Estimates of the population parameters

Parameter	Unit	Value	Relative Standard Error (%)
Fixed effects			
$Amyloid_0$	arbitrary	3.20	6.48
$\alpha_{removal}$	$\left(day \cdot \frac{mcg}{ml}\right)^{-1}$	0.126e-3	8.75
k_{repair}	day^{-1}	12.4e-3	6.64
β_1	arbitrary	9.37	8.21
VWD_{50}	arbitrary	0.418	3.89
$EG50$ (fixed)	arbitrary	1.00	
pow	-	3.72	5.5
$BGTS_{max}$ (fixed)	-	60	
Standard deviations of the random effects			
$\omega_{Amyloid_0}$	arbitrary	0.405	12.9
$\omega_{\alpha_{removal}}$	$log\left((day \cdot \frac{mcg}{ml})^{-1}\right)$	0.655	9.45
$\omega_{k_{repair}}$	$log(day^{-1})$	0.446	12.1
Standard deviation of the residual error			
a	-	2.83	4.63

Supplementary Table 3. Summary of the selected ARIA-E cases

ARIA-E case	APOE e4 status	Dosing regimen	Time of first ARIA-E [week]	Magnitude of first ARIA-E [BGTS]	Dose at first ARIA-E [mg]	Time of recurrent ARIA-E [week]	Magnitude of recurrent ARIA-E [BGTS]	Dose at recurrent ARIA-E [mg]
1	homozygous	4	22	10	1200	N/A	N/A	N/A
2	homozygous	4	13	6	900	N/A	N/A	N/A
3	heterozygous	1	30	6	450	61	9	900
4	heterozygous	2	14	20	450	52	12	900

The time is given with respect to the start of OLE treatment for all ARIA-E cases. The dosing regimens are given in Supplementary Table 1. The first ARIA-E refers to the first detected ARIA-E that required dose adjustments. ARIA-E case 1 experienced the first ARIA-E (mild severity; BGST =1) that did not require dose adjustments at week 12.

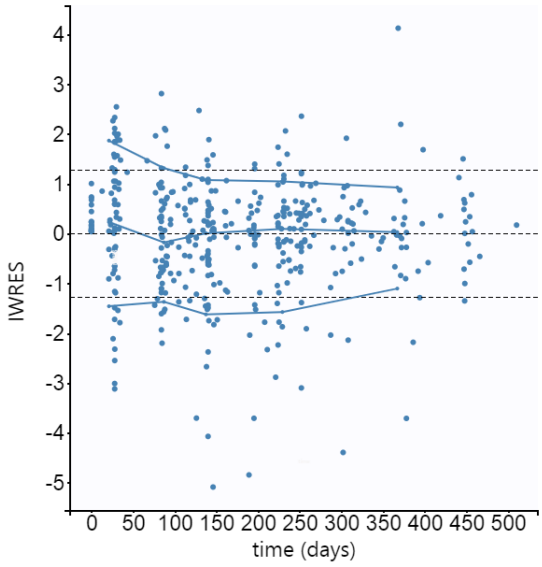

Supplementary Figure 1. Scatter plot of the residuals generated by the PK model used to predict the drug concentration in plasma for the ARIA-E cases from the SR/MR OLE studies. IWRES, individual weighted residuals. The solid lines represent the empirical (10th, 50th and 90th) percentiles, while the dotted lines represent the predicted (10th, 50th and 90th) percentiles.

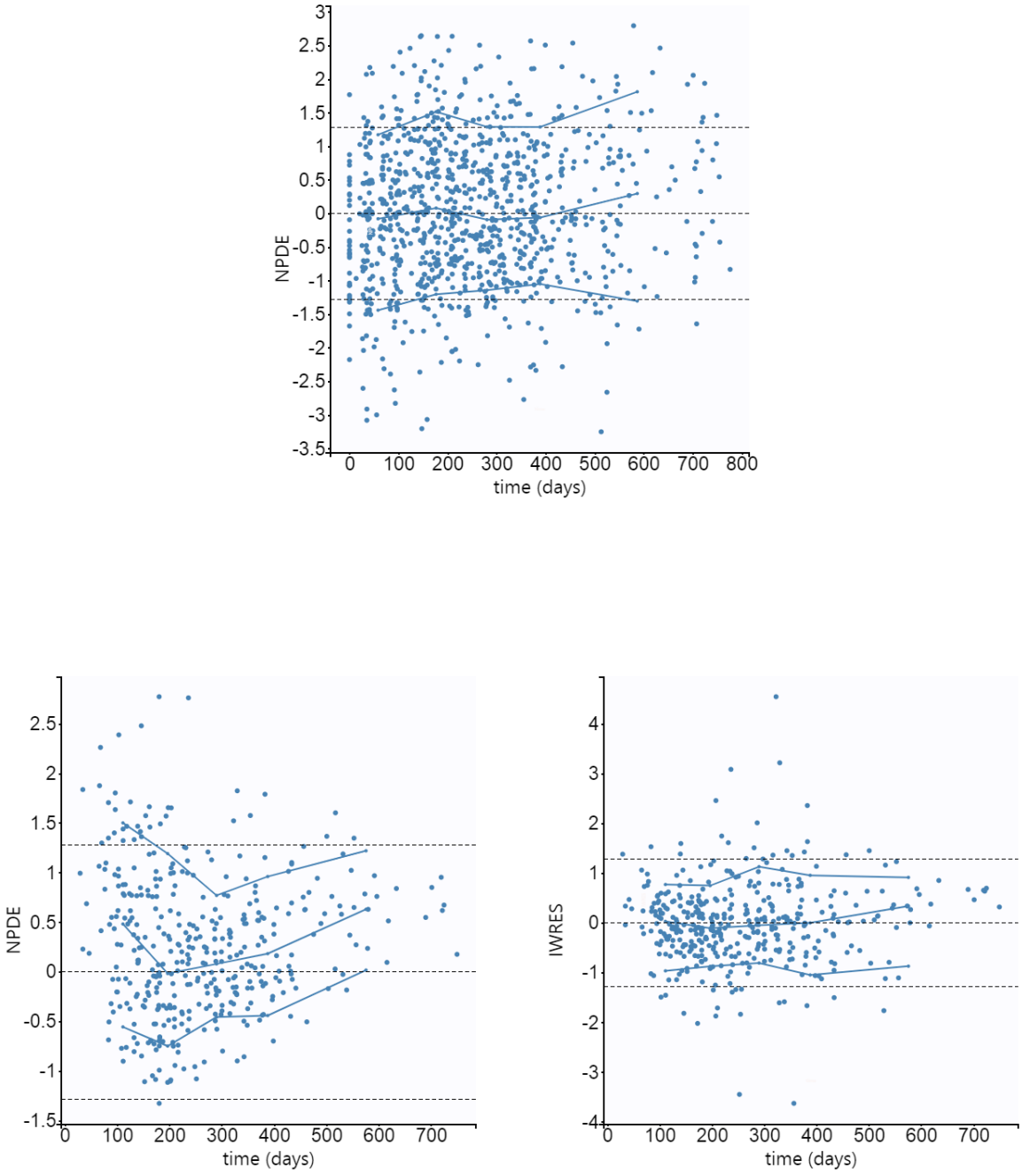

Supplementary Figure 2. Scatter plots of the residuals generated by part one (top panel) and part two (bottom panel) of the two-part PD model used to predict the probability of ARIA-E occurrence and the ARIA-E magnitude (given by BGTS), respectively. NPDE, normalized prediction distribution errors; IWRES, individual weighted residuals. The solid lines represent the empirical (10th, 50th and 90th) percentiles, while the dotted lines represent the predicted (10th, 50th and 90th) percentiles.

REFERENCES

[1] Barkhof F, Daams M, Scheltens P, Brashear HR, Arrighi HM, Bechten A, et al. An MRI Rating Scale for Amyloid-Related Imaging Abnormalities with Edema or Effusion 2013.
[2] Bechten A, Wattjes MP, Purcell DD, Aliaga ES, Daams M, Brashear HR, et al. Validation of an MRI Rating Scale for Amyloid-Related Imaging Abnormalities. J Neuroimaging 2017;27:318–25. https://doi.org/10.1111/jon.12422.
[3] Retout S, Gieschke R, Serafin D, Weber C, Frey N, Hofmann C. Disease Modeling and Model-Based Meta-Analyses to Define a New Direction for a Phase III Program of Gantenerumab in Alzheimer's Disease. Clin Pharmacol Ther 2022. https://doi.org/10.1002/cpt.2535.
[4] Farewell VT, Long DL, Tom BDM, Yiu S, Su L. Two-Part and Related Regression Models for Longitudinal Data. Annu Rev Stat Appl 2017;4:283–315. https://doi.org/10.1146/annurev-statistics-060116-054131.
[5] Salloway S, Chalkias S, Barkhof F, Burkett P, Barakos J, Purcell D, et al. Amyloid-Related Imaging Abnormalities in 2 Phase 3 Studies Evaluating Aducanumab in Patients With Early Alzheimer Disease. Jama Neurol 2022;79. https://doi.org/10.1001/jamaneurol.2021.4161.
[6] Muralidharan KK, Karumanchi S, Kowalski KG, Burkett P, Chapel S, Rajagovindan R, et al. A time-to-event exposure-response model for amyloid-related imaging abnormalities following administration of aducanumab to subjects with early alzheimer's disease. J Clin Pharmacol 2022. https://doi.org/10.1002/jcph.2047.
[7] Ostrowitzki S, Lasser RA, Dorflinger E, Scheltens P, Barkhof F, Nikolcheva T, et al. A phase III randomized trial of gantenerumab in prodromal Alzheimer's disease. Alzheimer's Res Ther 2017;9:95. https://doi.org/10.1186/s13195-017-0318-y.
[8] Johnson KA, Gregas M, Becker JA, Kinnecom C, Salat DH, Moran EK, et al. Imaging of amyloid burden and distribution in cerebral amyloid angiopathy. Ann Neurol 2007;62:229–34. https://doi.org/10.1002/ana.21164.
[9] Gurol ME, Becker JA, Fotiadis P, Riley G, Schwab K, Johnson KA, et al. Florbetapir-PET to diagnose cerebral amyloid angiopathy. Neurology 2016;87:2043–9. https://doi.org/10.1212/wnl.0000000000003197.
[10] McCarter S, Lesnick TG, Lowe V, Mielke MM, S ECMH, Rabinstein AA, et al. Cerebral Amyloid Angiopathy Pathology and Its Association With Amyloid-β PET Signal. Neurology 2021:10.1212/WNL.0000000000012770. https://doi.org/10.1212/wnl.0000000000012770.
[11] Sperling RA, Jack CR, Black SE, Frosch MP, Greenberg SM, Hyman BT, et al. Amyloid-related imaging abnormalities in amyloid-modifying therapeutic trials: Recommendations from the Alzheimer's Association Research Roundtable Workgroup. Alzheimer's Dementia 2011;7:367–85. https://doi.org/10.1016/j.jalz.2011.05.2351.
[12] Boncoraglio GB, Piazza F, Savoiardo M, Farina L, DiFrancesco JC, Prioni S, et al. Prodromal Alzheimer's Disease Presenting as Cerebral Amyloid Angiopathy-Related Inflammation with Spontaneous Amyloid-Related Imaging Abnormalities and High Cerebrospinal Fluid Anti-Aβ Autoantibodies. J Alzheimer's Dis 2015;45:363–7. https://doi.org/10.3233/jad-142376.
[13] Piazza F, Winblad B. Amyloid-Related Imaging Abnormalities (ARIA) in Immunotherapy Trials for Alzheimer's Disease: Need for Prognostic Biomarkers? J Alzheimer's Dis 2016;52:417–20. https://doi.org/10.3233/jad-160122.
[14] Antolini L, DiFrancesco JC, Zedde M, Basso G, Arighi A, Shima A, et al. Spontaneous ARIA-like Events in Cerebral Amyloid Angiopathy–Related Inflammation: A Multicenter Prospective Longitudinal Cohort Study. Neurology 2021:10.1212/WNL.0000000000012778. https://doi.org/10.1212/wnl.0000000000012778.
[15] Sveikata L, Charidimou A, Viswanathan A. Vessels Sing Their ARIAs: The Role of Vascular Amyloid in the Age of Aducanumab. Stroke 2022;53:298–302. https://doi.org/10.1161/strokeaha.121.036873.